Computational discovery of ferromagnetic semiconducting single-layer $CrSnTe_3$

Houlong L. Zhuang,[1,*] Yu Xie,[1] P. R. C. Kent,[1,2] and P. Ganesh[1]

[1]*Center for Nanophase Materials Sciences, Oak Ridge National Laboratory, Bethel Valley Road, Oak Ridge, Tennessee 37831, USA*

[2]*Computer Science and Mathematics Division, Oak Ridge National Laboratory, Bethel Valley Road, Oak Ridge, Tennessee 37831, USA*

(Received 6 October 2014; revised manuscript received 30 March 2015; published 6 July 2015)

Despite many single-layer materials being reported in the past decade, few of them exhibit magnetism. Here we perform first-principles calculations using accurate hybrid density functional methods (HSE06) to predict that single-layer $CrSnTe_3$ (CST) is a ferromagnetic semiconductor, with band gaps of 0.9 and 1.2 eV for the majority and minority spin channels, respectively. We determine the Curie temperature as 170 K, significantly higher than that of single-layer $CrSiTe_3$ (90 K) and $CrGeTe_3$ (130 K). This is due to the enhanced ionicity of the Sn-Te bond, which in turn increases the superexchange coupling between the magnetic Cr atoms. We further explore the mechanical and dynamical stability and strain response of this single-layer material for possible epitaxial growth. Our study provides an intuitive approach to understand and design single-layer magnetic semiconductors for a wide range of spintronics and energy applications.

DOI: 10.1103/PhysRevB.92.035407 PACS number(s): 75.50.Pp, 73.20.At, 75.70.−i, 75.30.−m

I. INTRODUCTION

Single-layer materials have attracted significant attention in the last decade owing to a wealth of interesting properties [1]. Electron spins in a single-layer material provide an additional degree of freedom to tailor their properties for spintronics applications [2]. Indeed, the occurrence of magnetic ordering in single-layer materials on its own is of great interest [3]. The Mermin-Wagner theorem states that long-range magnetic ordering is absent in an isotropic Heisenberg system when its dimension is less than or equal to two [4]. However, there exist two well-known exceptions of the theorem. First, spins in a two-dimensional (2D) system could form a vortex state resulting from the so-called Kosterlitz-Thouless transition [5]. The recently predicted single-layer K_2CuF_4 by Sach *et al.* lies in this category [6]. Second, the spins in the 2D system are constrained to only one direction, i.e., Ising-like spins. Indeed, inelastic neutron scattering measurements have revealed a gapped magnetic fluctuation in the layered $Cr_2Si_2Te_6$ compound, consistent with a 2D Ising-like nature for the spins [7].

In addition to the magnetic ordering, semiconductor based spintronic devices require a candidate single-layer material to be semiconducting. However, we are presently unaware of such a single-layer material which has been experimentally shown to exhibit both an intrinsic ferromagnetic ordering as well as a semiconducting behavior. Surprisingly, despite growing efforts in searching for such single-layer materials by density-functional theory based computational tools [8], only a handful of single-layer materials including MnS_2 [9], $CrSiTe_3$ [10], and $CrGeTe_3$ [10] have been predicted to possess the important coexistence of ferromagnetic and semiconducting properties recently.

In this paper, through first-principles calculations, we report on single-layer $CrSnTe_3$ (CST), in the family of ferromagnetic semiconducting single-layer materials. We study the mechanical and dynamical stability of single-layer CST by calculating the elastic constants and phonon spectrum. We show that ferromagnetic single-layer CST is both mechanically and dynamically stable. The electronic band structures calculated with the Heyd-Scuseria-Ernzerhof (HSE06) hybrid-density functional reveal that ferromagnetic single-layer CST is simultaneously a semiconductor with spin-up and spin-down band gaps of 0.9 and 1.2 eV, respectively, tunable by biaxial strains. Moreover, based on Monte Carlo simulations of the 2D Ising model, we find that single-layer CST exhibits a higher Curie temperature than single-layer $CrSiTe_3$ and $CrGeTe_3$. We show that this chemical trend of increased T_C is related to the stronger ionic bonding in CST, which enhances the superexchange coupling between the magnetic Cr ions via the Te atoms, consistent with the Goodenough-Kanamori-Anderson rules.

II. METHODS

We perform the first-principles calculations within density-functional theory (DFT) using the projector augmented wave method as implemented in the plane-wave code VASP (version 5.3.3) [11–13]. For all calculations, a cutoff energy of 400 eV is used to expand the wave functions in plane waves, ensuring the convergence of the total energy to within 1 meV per formula unit. Because of the high computational cost of the calculations of elastic constants and phonon spectrum, we use the Perdew-Burke-Ernzerhof (PBE) exchange-correlation functional for these calculations [14]. For the calculations of electronic structure and magnetic exchange integral, we employ the Heyd-Scuseria-Ernzerhof (HSE06) hybrid density functional, which mixes 25% nonlocal exchange with the PBE functional reducing the self-interaction error [14,15]. The k-point sampling uses the Monkhorst-Pack scheme [16] and employs $9 \times 9 \times 1$ and $6 \times 6 \times 1$ Γ-centered meshes for the PBE and HSE06 functionals, respectively. A vacuum spacing of 15 Å is used to avoid the interactions between the layers. All the atoms in the supercells are fully relaxed with the convergence force set to 0.01 eV/Å.

We assume that single-layer CST occurs as the same crystal structure as a layer of bulk $CrXTe_3$ illustrated in Fig. 1 [7,17,18]. One unit cell of single-layer CST contains two Cr atoms, each of which is bonded to six nearest-neighboring

*zhuanghl@ornl.gov

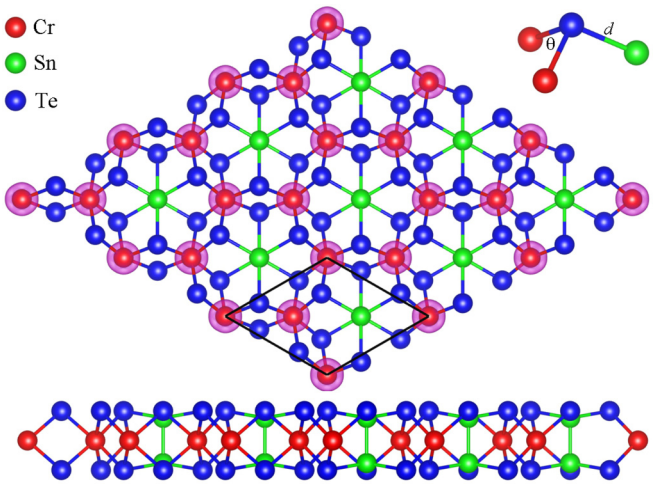

FIG. 1. (Color online) Top and side views of single-layer $CrSnTe_3$ structure. The solid black line encloses a unit cell of single-layer $CrSnTe_3$. The spin charge density is also shown with an isosurface of 0.025 e/Å^3.

Te atoms. In contrast, each of the two Sn atoms in the unit cell is only threefold coordinated to the Te atoms.

III. RESULTS

We first investigate the ground state magnetic ordering of single-layer CST. The energy difference between the ferromagnetic (FM) and Néel-type antiferromagnetic (AFM) ordered structures $E_{\mathrm{AFM}} - E_{\mathrm{FM}}$ are 106 and 102 meV calculated using the HSE06 and PBE functionals, respectively. This concludes that single-layer CST should exhibit FM ordering in the ground state, similar to the recently reported single-layer $CrSiTe_3$ and $CrGeTe_3$ [10]. Since the FM single-layer CST is more stable, we henceforth refer to single-layer CST as the one with this type of magnetic ordering.

We then study the mechanical stability of single-layer CST by calculating its two independent elastic constants,

$$C_{11} = \frac{1}{A_0} \cdot \frac{\partial^2 E}{\partial \epsilon_{11}^2} \quad \text{and} \quad C_{12} = \frac{1}{A_0} \cdot \frac{\partial^2 E}{\partial \epsilon_{11} \partial \epsilon_{12}}. \qquad (1)$$

E in Eq. (1) is the total energy of a unit cell employed for the calculations, and A_0 is the equilibrium area of a single-layer CST unit cell. We find that $C_{11} = 60$ N/m and $C_{12} = 17$ N/m, respectively, which clearly satisfy the Born stability criterion for single-layer materials, i.e., $(C_{11} - C_{12}) > 0$ [19].

We next consider the dynamical stability of single-layer CST by computing its phonon spectrum, which is obtained through post-processing the force constants of a $3 \times 3 \times 1$ supercell generated based on the finite-displacement method [20]. Figure 2 shows the phonon spectrum of single-layer CST with a prominent feature of the abundant flat phonon bands, which appears to be common in the phonon spectra of similar compounds such as $MnPSe_3$ [21]. More importantly, we observe all phonon frequencies are real, confirming the dynamical stability of single-layer CST.

To determine whether single-layer CST is semiconducting similar to single-layer $CrSiTe_3$ and $CrGeTe_3$ [10], we characterize its band structures using the HSE06 functional and

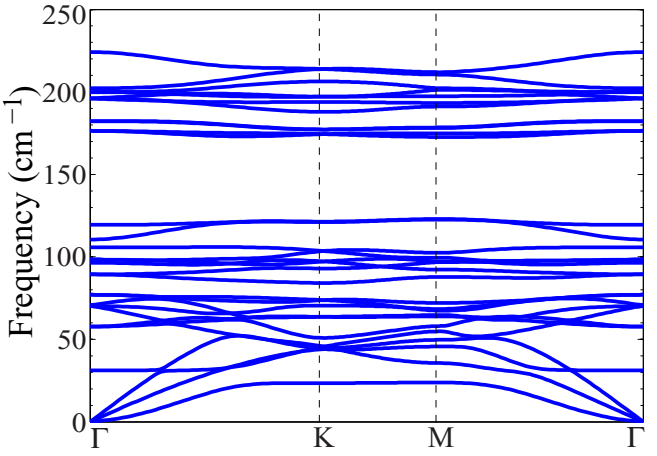

FIG. 2. (Color online) Calculated phonon spectrum of single-layer $CrSnTe_3$.

the correspondingly relaxed atomic configurations. Figure 3 shows the spin-polarized band structures of single-layer CST, revealing that it is semiconducting with indirect fundamental band gaps of 0.87 and 1.19 eV, respectively. These band gaps are smaller than many other single-layer materials such as MoS_2 with a band gap of 1.9 eV [22]. Therefore, single-layer CST may not be similarly useful for solar-energy conversion applications. However, the band gaps are as sizable as bulk silicon's, promising single-layer CST applications in electronic devices. Note that without using the hybrid density functional, the PBE spin-up and spin-down band gaps are merely 0.44 and 0.30 eV, respectively.

To understand the bonding characteristics of single-layer CST, we analyze the spin-resolved density of states within the energy window ranging from −3 to 3 eV with reference to the valence band maximum. Due to the D_{3d} symmetry of the trigonal antiprismic $CrTe_6$ complexes, we decompose the Cr 4d orbitals into the $A_{1g}(d_{z^2})$, $E_g(d_{x^2-y^2},d_{xz})$, and $E_g(d_{xy},d_{yz})$ ones. As can be seen in Fig. 4(a), the entire energy window is dominated by the Te 5p and Cr 4d orbitals confirming that the important superexchange interaction between the Cr 4d

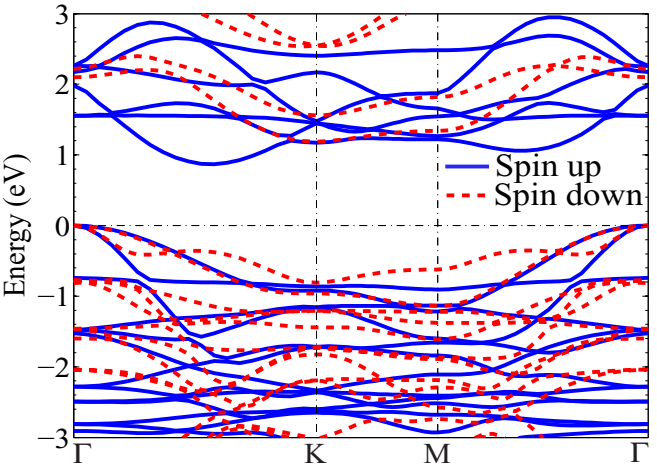

FIG. 3. (Color online) Spin-resolved band structures of single-layer $CrSnTe_3$ calculated with the HSE06 functional.

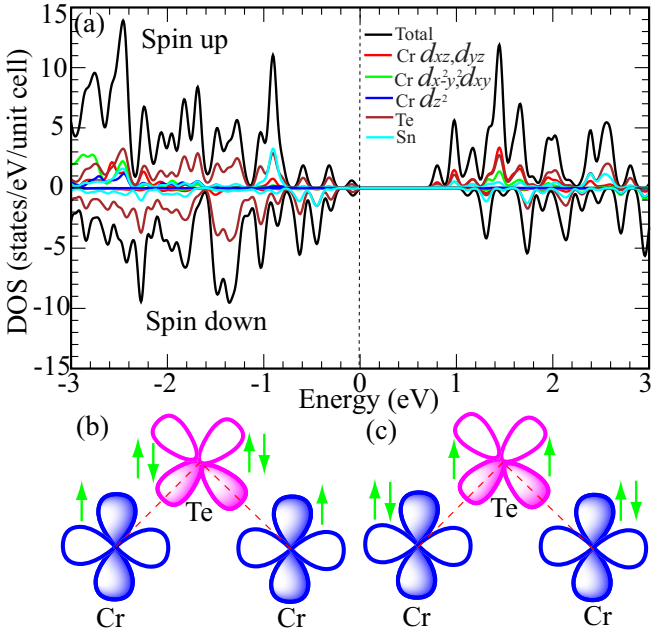

FIG. 4. (Color online) (a) Spin-resolved density of states of single-layer $CrSnTe_3$ calculated using the HSE06 functional. (b) and (c) Illustrations of the superexchange mechanism in single-layer $CrXTe_3$ (X= Sn, Ge, and Si).

orbitals is mediated by the neighboring Te $5p$ orbitals [18]. The spin charge density plotted in Fig. 1 shows significant orbital localization around the Cr atoms. In addition, the distance between two nearest-neighboring Cr atoms is as large as 4.05 Å, therefore the direct exchange between these two atoms becomes rather unlikely.

Superexchange interaction usually gives rise to antiferromagnetic ordering, especially for systems with cation-anion-cation bond angles of 180°. This is understandable from the well-known Goodenough-Kanamori-Anderson (GKA) rules [23–25]. However, the GKA rules also provide explanations for systems with cation-anion-cation bond angles of 90°, which indeed often favor weak ferromagnetic ordering. Single-layer $CrXTe_3$ belongs to the latter case, since the Cr-Te-Cr bond angles are all close to 90°, which can be seen from Table I. Phenomenally from the GKA rules [26], each of the two Te-pσ orbitals sketched in Fig. 4(b) are orthogonal to the d orbitals of the neighboring Cr ions. This leads to zero overlap integral S. According to the Heitler-London model [27], the

TABLE I. Lattice constant (a_0), X-Te bond length (d), Cr-Te-Cr bond angle (Θ), exchange integral J, and magnetocrystalline anisotropy energy (MAE) of single-layer $CrXTe_3$ (X= Sn, Ge, and Si) with the ferromagnetic ordering calculated using the HSE06 functional and a $6 \times 6 \times 1$ k-point grid ensuring the MAE convergence to within 6 μeV/f.u.

Materials	a_0 (Å)	d (Å)	Θ (deg)	J (meV)	MAE (μeV/f.u.)
$CrSnTe_3$	7.01	2.75	92.63	3.92	69
$CrGeTe_3$	6.83	2.58	90.33	3.07	220
$CrSiTe_3$	6.77	2.51	89.31	2.10	419

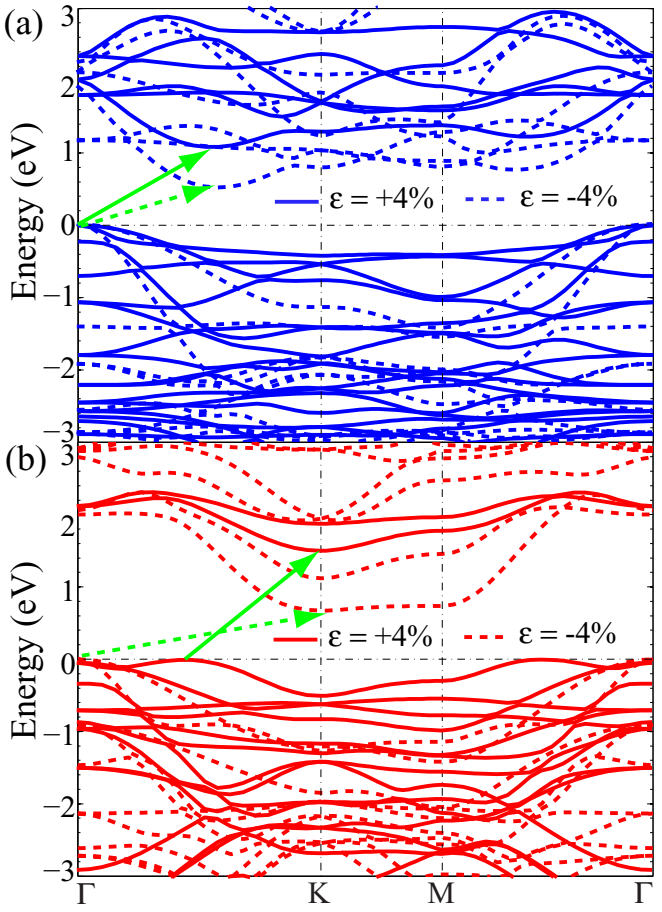

FIG. 5. (Color online) Strain effects on (a) spin-up and (b) spin-down band structures of single-layer $CrSnTe_3$. To aid the visualizations of band gaps, each pair of valence band maximum and conduction band minimum is connected by an arrow.

exchange integral can be written as $J = 2k + 4\beta S$, where k and β are potential exchange and hopping integral, respectively. Due to the zero S, J is reduced to $2k$, which is positive because of Hund's rule reflected by the parallel spins as shown in Fig. 4(c) for the two Te-pσ orbitals. As a result, single-layer $CrXTe_3$ all adopt ferromagnetic ordering.

Similar to the other single-layer materials such as MoS_2 [28,29], the band gaps of single-layer CST can be tuned by mechanical biaxial strains. Figure 5 shows the HSE06 band structures of single-layer CST subjected to strains $\epsilon = \pm 4\%$, corresponding to tensile and compressive strains, respectively. Tensile strain increases both the spin-up and spin-down band gaps, similar to what is seen in 3D bulk crystals. For example, at $\epsilon = 4\%$, the spin-up and spin-down band gaps are widened to 1.08 and 1.51 eV, respectively. Moreover, the strain switches the location of valence band maximum of the spin-down band structure from the Γ point to one between the Γ and K points. On the contrary, compressive strains reduce the corresponding band gaps to 0.50 and 0.67 eV at the $\epsilon = -4\%$. These strain effects on band gaps provide a useful route to control the band gap by design via epitaxy.

The Curie temperature T_C is a key design parameter of a ferromagnetic single-layer material. We adopt two methods to compute the T_C of ferromagnetic single-layer CST. The first

one is based on the Weiss molecular-field theory [30], where T_C is calculated as [31]

$$T_C = \frac{2zJS(S+1)}{3K_B}. \quad (2)$$

Here, $z = 3$ is the number of nearest-neighboring Cr atoms of a Cr atom in single-layer CST, $S = 3/2$ is the spin of each Cr atom, and K_B is the Boltzmann constant. The S value is consistent with the calculated magnetic moment of 3 μ_B using the HSE06 functional. To obtain the unknown term J in Eq. (2), we first calculate the exchange energy E_{ex} between the two Cr atoms in a unit cell of single-layer CST defined as

$$E_{ex} = -2zJS^2. \quad (3)$$

The energies of a single-layer CST unit cell with the FM and AFM orderings, E_{FM} and E_{AFM}, can be regarded as $E_{FM/AFM} = E_0 \pm E_{ex}$ [9], where E_0 is the energy of a single-layer CST unit cell without spin polarizations. Therefore, the energy difference between E_{FM} and E_{AFM} gives $2E_{ex}$. As a result, J is determined with the HSE06 functional as 3.92 meV. The PBE functional in our work leads to similar J of 3.79 meV. Further from Eq. (2), we obtain a Curie temperature of 341 K with the HSE06 functional and a slightly smaller temperature of 330 K with the PBE functional.

The molecular-field theory generally overestimates the Curie temperature [9]. Two common models including the 2D Ising model [32] and the Heisenberg model [10] are used in the literature to obtain a more accurate Curie temperature of single-layer materials, and a valid model selection is dependent on the magnetocrystalline anisotropic energy (MAE) of a system. With the HSE06 functional, we calculate the MAE of single-layer CrXTe$_3$, which is defined [33] as the energy difference when the magnetic moments of X atoms are constrained in the x and z axis, respectively. Based on this definition, positive MAE denotes that the magnetization along the z axis is energetically favorable.

Table I lists the calculated MAE results ranging from 69 to 419 μeV/f.u. for all three CrXTe$_3$. These values are of considerable magnitude. For example, the MAE in common cubic transition metals such as Fe, Co, and Ni is merely 1.3–2.7 μeV/atom [31] and in the well-known FeRh/MgO heterostructure that undergoes a complete spin re-orientation with temperature, the maximum value is around 45 μeV/f.u. [34]. Decrease in MAE as X changes from Si to Sn emphasizes the main conclusion in our paper that the bonding becomes more ionic as we go down the periodic table, i.e., more isotropic compared to the covalently bonded CrSiTe$_3$.

Irkhin *et al.* [35] considered the effect of magnetic anisotropy on Curie temperature of two-dimensional magnets and showed that there exists a logarithmic correction factor, which is proportional to $\log(T_C/\mathrm{MAE}/K_B)$. Here, T_C is predicted based on the molecular-field theory. We estimate this factor for all three CrXTe$_3$ to be significantly greater than one, therefore lowering T_C.

Sizable MAE implies that magnetocrystalline anisotropy in single-layer CrXTe$_3$ is significant. Therefore our large calculated MAE values show that the z axis is the easy one for the magnetization in the CrXTe$_3$ family of materials. Indeed, a previous experiment has shown that bulk CrSiTe$_3$ is a quasi-2D Ising ferromagnet [7]. Overall, it is more accurate

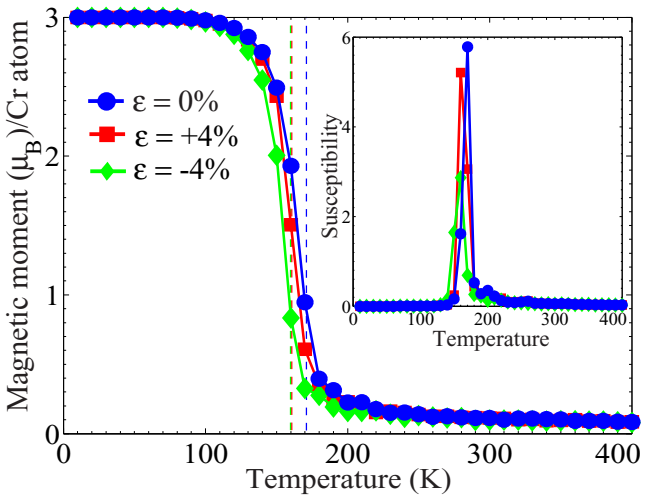

FIG. 6. (Color online) Magnetic moment per Cr atom of single-layer CrSnTi$_3$ under different biaxial strains as a function of temperature. The relation between magnetic susceptibility and temperature is shown in the inset.

to use the 2D Ising model than the isotropic Heisenberg model to describe the spin coupling in single-layer CrSiTe$_3$. As a matter of fact, applying the isotropic Heisenberg model to a 2D ferromagnetic system is against the Mermin-Wagner theorem, which claims the absence of long-range magnetic ordering at nonzero temperature in an isotropic Heisenberg system. In addition, large MAE makes the Kosterliz-Thouless transition unlikely to take place in single-layer CrXTe$_3$, since the magnetic moments are not favorable to lie in the xy plane.

According to the above discussion to obtain more accurate T_C of single-layer CST, we carry out Monte Carlo (MC) simulations based on the 2D Ising model with the Hamiltonian of $H = -\sum_{ij} JS_i^z S_j^z$, where $S_{i/j}^z$ is the spin parallel or antiparallel to the z direction. Only the nearest-neighboring exchange interactions are considered. We use a $100 \times 100 \times 1$ supercell as well as the periodic boundary conditions for the MC simulations. The simulations are run for one million MC steps, and the total magnetic moments of the supercell are measured every 1000 steps. Figure 6 shows the magnetic moment per Cr atom and magnetic susceptibility as a function of temperature. The T_C extracted from the figure is around 170 K using the HSE06 functional. For the PBE functional, the T_C is estimated to be 160 K, which is again marginally different from the HSE06 result.

Using the same methodology, we obtain the T_C of single-layer CrGeTe$_3$ and CrSiTe$_3$ from the variation of their magnetic moment and magnetic susceptibility with temperature as shown in Fig. 7. The T_C of single-layer CrGeTe$_3$ and CrSiTe$_3$ are determined as 130 K and 90 K, respectively, which are both lower than the T_C of single-layer CST, suggesting that single-layer CST is more promising for practical spintronics applications.

Surprisingly, our calculated T_C for single-layer CrSiTe$_3$ and CrGeTe$_3$ are significantly larger than the values reported in Ref. [10], although the reference uses larger exchange integrals for the Monte Carlo simulations. Using the mean field theory along with the exchange integral from Ref. [10], e.g., 3.38 meV

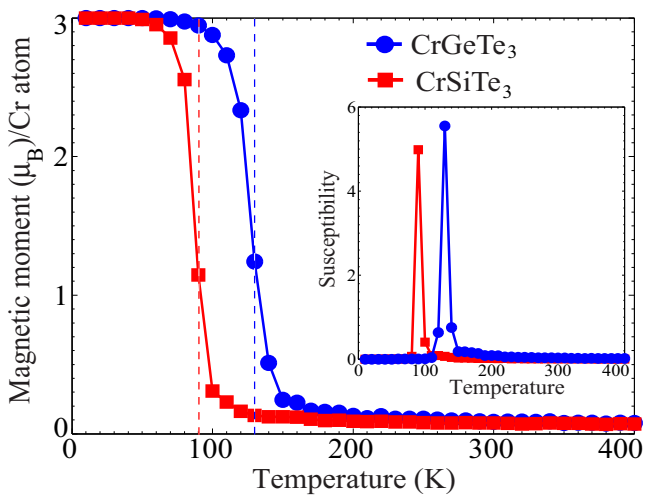

FIG. 7. (Color online) Magnetic moment per Cr atom of single-layer $CrGeTi_3$ and $CrSiTi_3$ as a function of temperature. The inset shows the variation of magnetic susceptibility with temperature.

for single-layer $CrSiTe_3$, the resulting T_C is 294 K, which is significantly higher than our estimated value of 183 K.

The increasing T_C from $CrSiTe_3$ and $CrGeTe_3$ to $CrSnTe_3$ is also consistent with the decreasing X-Te (X = Sn, Ge, and Si) bond lengths that leads to an increasing Cr-Te-Cr bond angle, as shown in Table I, indicating an interesting correlation between the structure and the Curie temperature.

To understand the enhanced T_C in single-layer CST, we analyze the nature of the X-Te bonds by comparing the electron localization function (ELF) of all three materials as illustrated in Fig. 8. We observe that there are almost no overlapping electron pockets along the Sn-Te bond, revealing the key feature of ionic bonding. On the contrary, the electron clouds are more significant on the Ge-Te and Si-Te bonds, suggesting that they are covalent in nature. In other words, the ionicity of single-layer CST is the strongest among the three single-layer materials with increased electron density at the Te site, thereby leading to an increased super exchange coupling interaction between the Cr atoms via the Te atom. This correlation between the increased Cr-Te-Cr bond angle with an increase in the superexchange coupling is consistent with the GKA rules and explains why CST has the highest Curie temperature among these three compounds.

Finally, we study the strain effects on the Curie temperature of single-layer CST. Unlike the significant strain effects on band gaps, strains trivially affect the Curie temperature of single-layer CST. As seen from Fig. 6, applying 4% of tensile or compressive strain changes the critical temperature to around 160 K, which is almost the same as the unstrained case. This is because strain affects both the FM and AFM ordered single-layer CST at nearly the same rate consistent

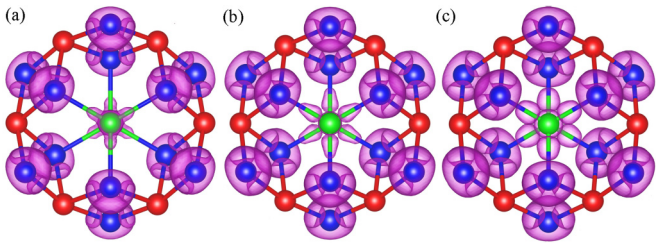

FIG. 8. (Color online) Electron localization functions of single-layer (a) $CrSnTe_3$, (b) $CrGeTe_3$, and (c) $CrSiTe_3$ with an isosurface of 1.5×10^{-4}.

with the recent study of CrXTe$_3$ [10]. As a consequence, the exchange integral is insignificantly affected by the strains.

IV. CONCLUSIONS

In summary, we have computationally predicted and characterized a single-layer semiconducting and ferromagnetic material $CrSnTe_3$. We show that single-layer CST is mechanically and dynamically stable. We further rationalize that CST shows a higher T_C than the remaining members of the CrXTe$_3$ family due to an increased superexchange coupling between Cr atoms due to the relatively enhanced ionicity of the Sn-Te bond. We expect our rational prediction to stimulate experimental interests in synthesizing this novel single-layer material. Nevertheless, one main concern is that the predicted Curie temperature (170 K) of single-layer CST is below room temperature, inevitably limiting its wide applications in spintronics devices. However, this will not hamper single-layer CST to potentially become a testing-ground material useful for fundamental physics studies. For example, bulk $CrGeTe_3$ is recently proposed as a candidate substrate for topological insulators due to its unique combination of semiconducting and ferromagnetic properties [36]. Meanwhile, searching for other CST-like (e.g., MPY_3, M = Mn, Fe, Ni; Y = S, Se) single-layer ferromagnetic semiconducting materials with higher Curie temperatures is underway through a high-throughput data-mining technique.

ACKNOWLEDGMENTS

This research was conducted at the Center for Nanophase Materials Sciences, which is a DOE Office of Science User Facility. A part of this research used computational resources of the Texas Advanced Computing Center under Contract No. TG-DMR140067. A part of this material is based upon work performed using computational resources supported by the University of Tennessee and Oak Ridge National Laboratory's Joint Institute for Computational Sciences (http://www.jics.utk.edu). We thank Kai Xiao and Richard Hennig for helpful discussions.

[1] M. Xu, T. Liang, M. Shi, and H. Chen, Chem. Rev. **113**, 3766 (2013).
[2] H. Kabbour, R. David, A. Pautrat, H.-J. Koo, M.-H. Whangbo, G. Andre, and O. Mentre, Angew. Chem., Int. Ed. **51**, 11745 (2012).
[3] C. A. F. Vaz, J. A. C. Bland, and G. Lauhoff, Rep. Prog. Phys. **71**, 056501 (2008).
[4] N. D. Mermin and H. Wagner, Phys. Rev. Lett. **17**, 1133 (1966).
[5] J. M. Kosterlitz and D. J. Thouless, J. Phys. C: Solid State Phys. **6**, 1181 (1973).

[6] B. Sachs, T. O. Wehling, K. S. Novoselov, A. I. Lichtenstein, and M. I. Katsnelson, Phys. Rev. B **88**, 201402 (2013).
[7] V. Carteaux, F. Moussa, and M. Spiesser, Europhys. Lett. **29**, 251 (1995).
[8] S. Lebègue, T. Björkman, M. Klintenberg, R. M. Nieminen, and O. Eriksson, Phys. Rev. X **3**, 031002 (2013).
[9] M. Kan, S. Adhikari, and Q. Sun, Phys. Chem. Chem. Phys. **16**, 4990 (2014).
[10] X. Li and J. Yang, J. Mater. Chem. C **2**, 7071 (2014).
[11] G. Kresse and J. Furthmüller, Phys. Rev. B **54**, 11169 (1996).
[12] P. E. Blöchl, Phys. Rev. B **50**, 17953 (1994).
[13] G. Kresse and D. Joubert, Phys. Rev. B **59**, 1758 (1999).
[14] J. P. Perdew, K. Burke, and M. Ernzerhof, Phys. Rev. Lett. **77**, 3865 (1996).
[15] J. Heyd, G. E. Scuseria, and M. Ernzerhof, J. Chem. Phys. **118**, 8207 (2003).
[16] H. J. Monkhorst and J. D. Pack, Phys. Rev. B **13**, 5188 (1976).
[17] V. Carteaux, G. Ouvrard, J. Grenier, and Y. Laligant, J. Magn. Magn. Mater. **94**, 127 (1991).
[18] V. Carteaux, D. Brunet, G. Ouvrard, and G. Andre, J. Phys.: Condens. Matter **7**, 69 (1995).
[19] H. L. Zhuang, M. D. Johannes, M. N. Blonsky, and R. G. Hennig, Appl. Phys. Lett. **104**, 022116 (2014).
[20] L. Chaput, A. Togo, I. Tanaka, and G. Hug, Phys. Rev. B **84**, 094302 (2011).
[21] M. Bernasconi, G. L. Marra, G. Benedek, L. Miglio, M. Jouanne, C. Julien, M. Scagliotti, and M. Balkanski, Phys. Rev. B **38**, 12089 (1988).
[22] K. F. Mak, C. Lee, J. Hone, J. Shan, and T. F. Heinz, Phys. Rev. Lett. **105**, 136805 (2010).
[23] J. B. Goodenough, Phys. Rev. **100**, 564 (1955).
[24] J. Kanamori, J. Appl. Phys. **31**, S14 (1960).
[25] P. Anderson, Phys. Rev. **115**, 2 (1959).
[26] P. A. Cox, *Transition Metal Oxides: An Introduction to their Electronic Structure and Properties* (Oxford University Press, New York, 2010).
[27] W. Heitler and F. London, Z. Phys. **44**, 455 (1927).
[28] J. Feng, X. Qian, C.-W. Huang, and J. Li, Nat. Photon. **6**, 866 (2012).
[29] H. J. Conley, B. Wang, J. I. Ziegler, R. F. Haglund, S. T. Pantelides, and K. I. Bolotin, Nano Lett. **13**, 3626 (2013).
[30] B. D. Cullity and C. D. Graham, *Introduction to Magnetic Materials* (Wiley-IEEE, New Jersey, 2008).
[31] S. V. Halilov, A. Y. Perlov, P. M. Oppeneer, A. N. Yaresko, and V. N. Antonov, Phys. Rev. B **57**, 9557 (1998).
[32] J. Zhou and Q. Sun, J. Am. Chem. Soc. **133**, 15113 (2011).
[33] A. Deák, E. Simon, L. Balogh, L. Szunyogh, M. dos Santos Dias, and J. B. Staunton, Phys. Rev. B **89**, 224401 (2014).
[34] A. Hierro-Rodriguez, R. Cid, M. Velez, G. Rodriguez-Rodriguez, J. I. Martin, L. M. Alvarez-Prado, and J. M. Alameda, Phys. Rev. Lett. **109**, 117202 (2012).
[35] V. Y. Irkhin, A. A. Katanin, and M. I. Katsnelson, Phys. Rev. B **60**, 1082 (1999).
[36] H. Ji, R. A. Stokes, L. D. Alegria, E. C. Blomberg, M. A. Tanatar, A. Reijnders, L. M. Schoop, T. Liang, R. Prozorov, K. S. Burch, N. P. Ong, J. R. Petta, and R. J. Cava, J. Appl. Phys. **114**, 114907 (2013).